
**Aerodynamics Laboratory (AE 312)**

# Low Speed Flow Past a Symmetric Airfoil

performed by

V S Harikrishna - 160010054

Laboratory Guide : Ashutosh
Instructor : Prof. Vineeth Nair

Department of Aerospace Engineering
Indian Institute of Technology, Bombay

January 2023

# Contents

# List of Figures



# List of Tables

# List of Symbols

| | |
|---|---|
| $\alpha$ | Angle of Attack |
| $C_a$ | Sectional coefficient of force along free-stream direction |
| $C_{d,f}$ | Sectional coefficient of skin-friction Drag calculated from experimental data |
| $C_{d,p}$ | Sectional coefficient of Pressure Drag calculated from experimental data |
| $C_{d,total}$ | Sectional coefficient of Total Drag calculated from experimental data |
| $C_{l_{th}}$ | Theoretical sectional coefficient of Lift obtained from the Thin Airfoil Theory |
| $C_l$ | Sectional coefficient of Lift calculated from experimental data |
| $C_{m,c/4_{th}}$ | Theoretical sectional coefficient of Quarter Chord Moment obtained from the Thin Airfoil Theory |
| $C_{m,c/4}$ | Theoretical sectional coefficient of Quarter Chord Moment calculated from experimental data |
| $C_{m,LE_{th}}$ | Theoretical sectional coefficient of Leading Edge Moment obtained from the Thin Airfoil Theory |
| $C_{m,LE}$ | Theoretical sectional coefficient of Leading Edge Moment calculated from experimental data |
| $C_n$ | Sectional coefficient of force along the direction normal to free-stream |
| $x_{ac}$ | Aerodynamic Center |
| $x_{cp}$ | x Coordinate Center of pressure |
| $z_l$ | z coordinates of Lower Surface of the Aerofoil |
| $z_u$ | z coordinates of Upper Surface of Aerofoil |

**Abstract**

The experiment was carried out in an attempt to observe and analyse the characteristics of low speed flow past a symmetric airfoil for high Reynolds number. The lift, drag and moment characteristics calculated for various angles of attack are analysed and their variation with angle of attack is computed numerically and their variation is compared with theoretical and existing valid computational data[10]. Based on the obtained data, the location of aerodynamic center ($x_{ac}$) is predicted and compared with theoretical and valid experimental data obtained[7] from literature. It was observed that while values of estimated drag and lift coefficients were close to their theoretical values, the moment coefficients show significant deviation from theoretical predictions at high angle of flow incidence due to the breakdown of fundamental assumptions of minimal flow perturbation and thin airfoil.

# 1 OBJECTIVES

1. To observe and study the working and operating procedures of a suction type wind tunnel.

2. To capture and analyse an in-compressible flow past a symmetric air foil in the high Reynolds' number ($R_e$) regime by measuring the pressure distribution along he surface of the airfoil.

3. To predict the sectional coefficients of lift ($C_l$), pitching moments about the leading edge ($C_{m,LE}$) and quarter chord point ($C_{m,c/4}$)

4. To estimate the location of aerodynamic center for thin symmetrical airfoils using the computed values of sectional coefficients of lift ($C_l$) and pitching moments about the quarter chord point ($C_{m,c/4}$)

# 2 INTRODUCTION TO AIRFOILS

## 2.1 Airfoils

An airfoil is a two dimensional shape that interacts with aerodynamic flows to generate significant forces both tangential and normal to the direction of flow. These forces are called aerodynamic forces[2]. The geometrical characteristics of a typical airfoil shape is shown in Fig. 1.

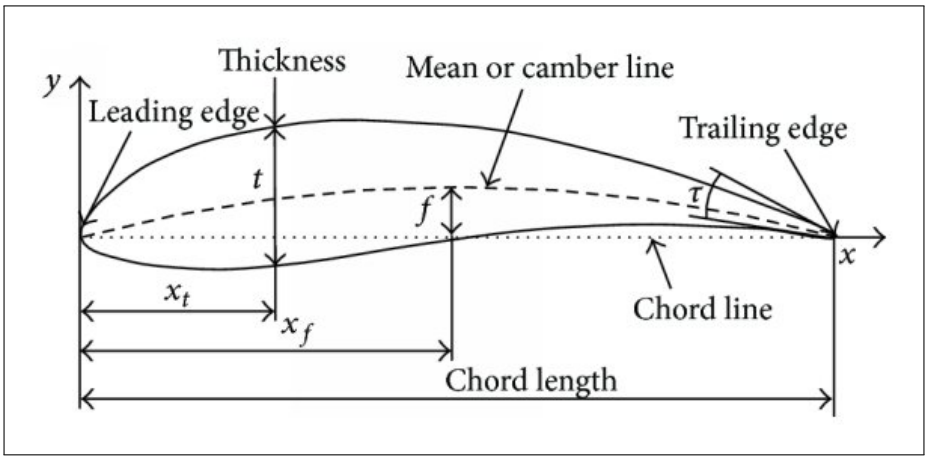


**Figure 1:** Airfoil nomenclature

The component of the net force normal to the direction of *mean chord* is termed $N'$ and that along the direction of free stream flow as $A'$. These forces are shown in Fig. 2. Another convention is to consider the components of net force parallel to the direction of free stream flow and perpendicular to it. The component parallel to the free stream direction of flow is termed as $D'$ and is called *drag*[6] force and the perpendicular component is termed as $L'$ and called *lift*[6] force. these are shown in Fig. 2. The force components are related by the following relations:

$$L' = N'cos\alpha - A'sin\alpha \tag{1}$$

$$D' = N'sin\alpha + A'cos\alpha \tag{2}$$

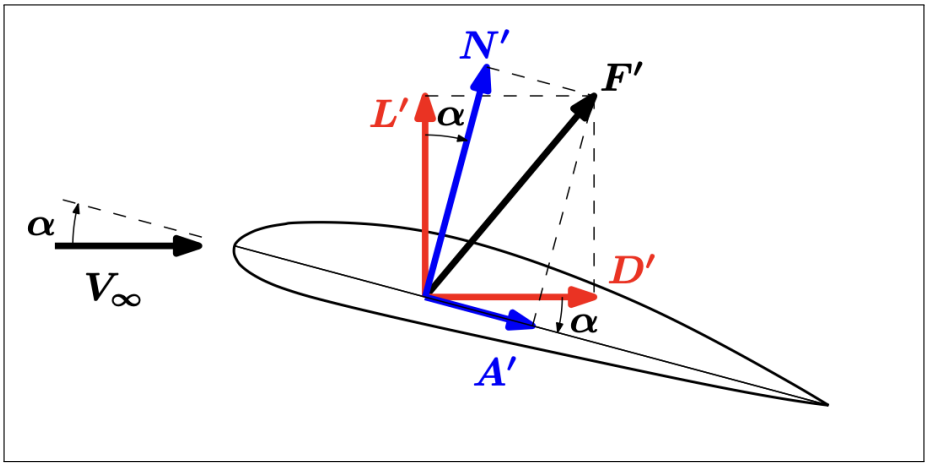


**Figure 2:** Airfoil forces and angle of incidence

Airfoils are named as per their geometrical characteristics. One such convention is the NACA 4-digit series naming convention[1]. It names the airfoil as the letter 'NACA' followed by four digits that characterise the airfoil's shape uniquely. In order to define the parameters which determine the four digits we define the coordinate system for points on the airfoil surface as shown in Fig. 3. Notice that the x axis shows the x-coordinates normalised with respect to the total chord length of the airfoil.

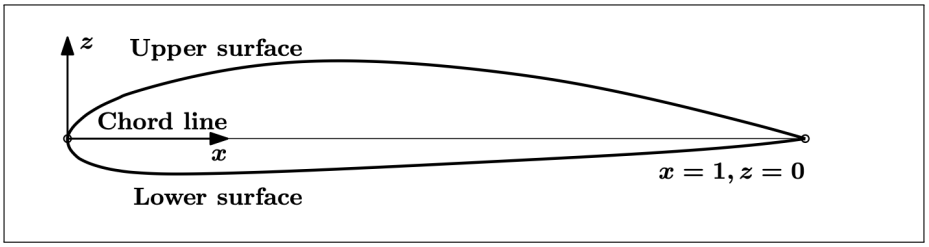


**Figure 3:** Coordinate system for NACA 4 series airfoil

The shape of an airfoil is characterised by its maximum *camber* ($m$) denoted by the first digit as a percentage of the chord length of the airfoil, The location of the maximum camber ($p$) denoted by the second digit in tenths of chord length, and its maximum *thickness* ($t$) denoted by the last two digits as percent of chord length. These parameters are shown in Fig. 4

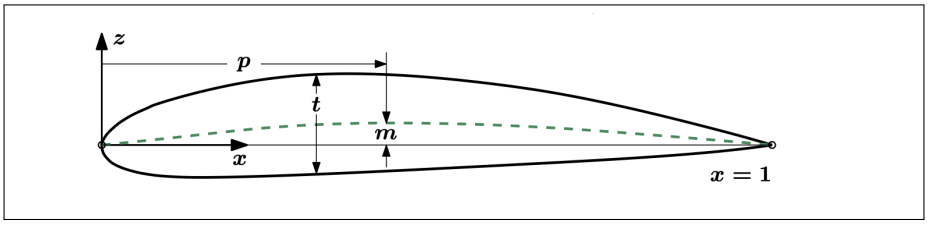


**Figure 4:** Coordinate system for NACA 4 series airfoil

In order to obtain the shape to the correct scale, one also needs the chord length as the above notation only gives the shape relative to a unit chord length. The equation of the top and bottom surface of a NACA airfoil can thus be represented as:

$$z_c = \begin{cases} \frac{m}{p^2}(2px - x^2), & 0 \le x \le p \\ \\ \frac{m}{1-p^2}((1-2p) + 2px - x^2), & p \le x \le 1 \end{cases} \tag{3}$$

The upper and lower surface coordinates can thus be found using the equation:

$$z_u = z_c + z_t \tag{4}$$

$$z_l = z_c - z_t \tag{5}$$

where $z_t$ is the airfoil half thickness at a given value of $x$ given by

$$z_t = 5t\left[0.2969\sqrt{x} - 0.1260x - 0.3516x^2 + 0.2843x^3 - 0.1015x^4\right] \tag{6}$$

The last coefficient may be replaced with $-0.1036$ in order to obtain a sharp, closed trailing edge without changing the overall shape of the airfoil too much [9].

For symmetric airfoils $z_c = 0$ and thus one only need to obtain the thickness distribution and chord length in order to characterise the airfoil shape.

### 2.1.1 Experimental Calculations

The aerodynamic characteristics of the airfoil can be calculated using experimental data through the given formulae [8].

$$C_n = \frac{1}{c}\left[\int_0^c (C_{p,l} - C_{p,u})dx + \int_0^c (C_{f,u}\frac{dz_u}{dx} - C_{f,l}\frac{dz_l}{dx})dx\right] \tag{7}$$

$$C_a = \frac{1}{c}\left[\int_0^c (C_{p,u}\frac{dz_u}{dx} - C_{p,l}\frac{dz_l}{dx})dx + \int_0^c (C_{f,u} + C_{f,l})dx\right] \tag{8}$$

$$C_{m.LE} = \frac{1}{c^2}\left[\begin{array}{c} \int_0^c (C_{p,u} - C_{p,l})xdx - \int_0^c \left(C_{f,u}\frac{dz_u}{dx} - C_{f,l}\frac{dz_l}{dx}\right)xdx \\ + \int_0^c \left(C_{p,u}\frac{dz_u}{dx} + C_{f,u}\right)z_u dx \int_0^c \left(C_{p,l}\frac{dz_l}{dx} + C_{f,l}\right)z_l dx \end{array}\right] \tag{9}$$

We apply the following simplifications:

1. Since the forces due to viscous effects are smaller compared to inertial forces, we assume that the coefficients $C_{f,u}$ and $C_{f,l}$ are small compared to the coefficients $C_{p,u}$ and $C_{p,l}$ respectively.

2. Since $C_{f,u}$ and $C_{f,l}$ are assumed to be small compared to the coefficients $C_{p,u}$ and $C_{p,l}$, we neglect the second order terms in eqn. (7), eqn. (8) and eqn. (9) to obtain eqn. (10), eqn. (11) and eqn. (12) respectively. Here we are assuming the derivatives $\frac{dz_u}{dx}$ and $\frac{dz_l}{dx}$ to be finite as airfoil is not consisting of any sharp edges on the upper and lower surface.

$$C_n = \frac{1}{c}\left[\int_0^c (C_{p,l} - C_{p,u})dx\right] \tag{10}$$

$$C_a = \frac{1}{c}\left[\int_0^c (C_{p,u}\frac{dz_u}{dx} - C_{p,l}\frac{dz_l}{dx})dx\right] \tag{11}$$

$$C_{m.LE} = \frac{1}{c^2}\left[\int_0^c (C_{p,u} - C_{p,l})xdx + \int_0^c \left(z_u C_{p,u}\frac{dz_u}{dx} - y_l C_{p,l}\frac{dz_l}{dx}\right)dx\right] \tag{12}$$

We compute the sectional coefficients of lift and pressure drag from the below expressions:

$$C_l = C_n \cos\alpha - C_a \sin\alpha \tag{13}$$

$$C_{d,p} = C_n \sin\alpha + C_a \cos\alpha \tag{14}$$

The sectional moment coefficient about the quarter chord point can be computed as follows:

$$C_{m,c/4} = \frac{1}{c^2}\left[\int_0^c (C_{p,u} - C_{p,l})(x - \frac{c}{4})dx + \int_0^c \left(z_u C_{p,u}\frac{dz_u}{dx} - z_l C_{p,l}\frac{dz_l}{dx}\right)dx\right] \tag{15}$$

The center of pressure, where the lift force is assumed to act is computed as shown below:

$$x_{cp} \approx -\frac{M'_{LE}}{L'}, \text{ at small } \alpha \tag{16}$$

From the velocity profile $u(z)$ in the airfoil wake, we can calculate the sectional coefficient of total drag.

$$C_{d,total} = \frac{2}{S}\left[\int_h^b \frac{u(z)}{V_\infty}\left(1 - \frac{u(z)}{V_\infty}\right)dz\right] \tag{17}$$

$$C_{d,f} = C_{d,total} - C_{d,p} \tag{18}$$

The integrals involved in above formulae are evaluated using the trapezoidal rule for integration, and the backward difference to compute derivatives as shown in the expressions below.

$$\int f(x)dx = \sum \frac{x_{i+1} - x_i}{2}[f(x_{i+1}) + f(x_i)] \tag{19}$$

$$\frac{df(x_i)}{dx} = \frac{f(x_i) - f(x_{i-1})}{x_i - x_{i-1}} \tag{20}$$

### 2.1.2 Theoretical Predictions

For thin symmetrical airfoils, the sectional coefficient of lift ($C_{l_{theory}}$) and the sectional coefficients of moment ($C_{m,LE_{theory}}$, $C_{m,c/4_{theory}}$) are computed as follows:

$$C_{l_{theory}} = 2\pi\alpha \tag{21}$$

$$C_{m,LE_{theory}} = -\left[\frac{C_{l_{theory}}}{4}\right] \tag{22}$$

$$C_{m,c/4_{theory}} = 0 \tag{23}$$

Using Thin Airfoil Theory, the location of center of pressure is obtained as :

$$x_{cp,theory} = -\frac{C_{m,LE_{theory}}}{C_{l_{theory}}} \tag{24}$$

## 2.2 Apparatus Used

1. NACA 0012 airfoil (with pressure ports for pressure measurement).
2. Wind tunnel
3. Pitot static probe
4. 2 channel selector boxes
5. Spirit level (angle setter)
6. Digital Manometer
7. Traverse (horizontal and vertical)

## 2.3 Experiment Setup

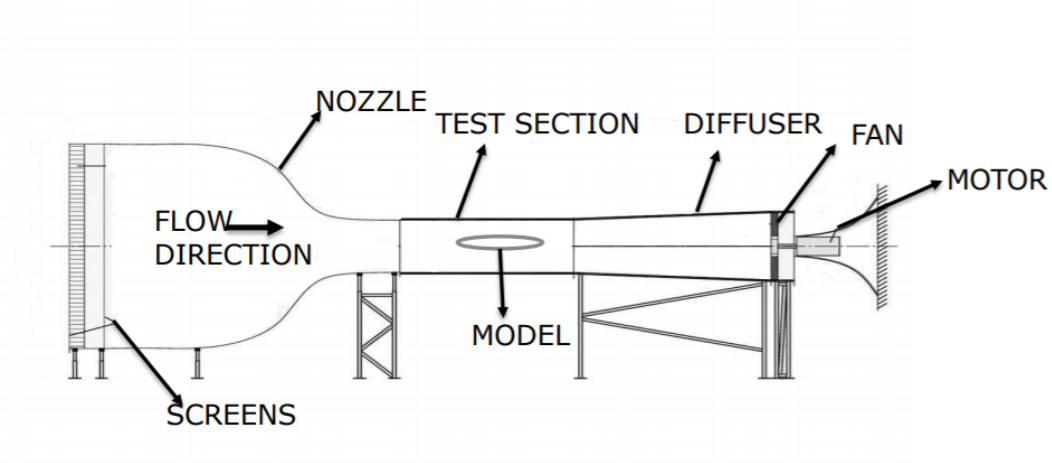


**Figure 5:** Wind Tunnel Setup

## 2.4 Wind Tunnel

The wind tunnel used is an open channel suction type wind tunnel. Two dimensional flow effects are eliminated through installing bell mount structures at inlet of the tunnel. Screens are placed upstream of the inlet to homogenize turbulence effects and eddy formation as flow enters the tunnel. Two screens one horizontal and one netted, are present for this purpose. The flow is accelerated through a 9:1 converging nozzle and desired speed is achieved by adjusting the motor RPM. Care is taken to place measurement devices away from walls where the flow is uniform and quasi-one-dimensional. The flow after the test section is decelerated through a diffuser before exiting through the fan manifold.

## 2.5 Airfoil Geometry

The airfoil used is the NACA 4-digit series airfoil designated as NACA 0012. It is a symmetric airfoil with no camber as indicated by the first digit. Since there is no camber, the location of maximum camber is set to zero as the second digit implies in the code. The maximum thickness is 12% of the chord length denoted by the last two digits of the airfoil. A plot of the airfoil is attached below comparing with the coordinated obtained from UIUC airfoil database [5].

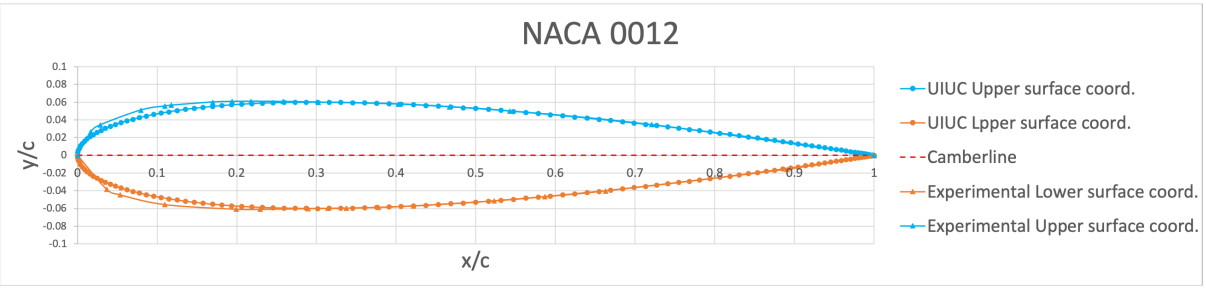


**Figure 6:** NACA 0012 Airfoil

| | | |
|---|---|---|
| Chord length ($c$) | = | 15 $cm$ |
| Span ($b$) | = | 2 $ft$ |
| Max. thickness to chord ratio ($t$) | = | 0.12 |
| Max. Camber to chord ratio ($m$) | = | 0 |
| Position of max camber as% chord ($p$) | = | 0 |
| Position of max thickness (% chord) | = | 30 |

### 2.6 Ambient Data and Associated errors

Day 1:

| Parameter | Measured value | Absolute error |
|---|---|---|
| $T_\infty$ | 296.16 $K$ | 0.1 $K$ |
| $P_\infty$ | 100760 $Pa$ | 10 $Pa$ |
| $\rho_\infty$ | 1.1759 $kg/m^3$ | -0.07969 $kg/m^3$ |
| $V_{\infty,test}$ | 17 $m/s$ | 0 $m/s$ |

Day 2:

| Parameter | Measured value | Absolute error |
|---|---|---|
| $T_\infty$ | 296.16 $K$ | 0.1 $K$ |
| $P_\infty$ | 100760 $Pa$ | 10 $Pa$ |
| $\rho_\infty$ | 1.1759 $kg/m^3$ | -0.07969 $kg/m^3$ |
| $V_{\infty,test}$ | 17 $m/s$ | 0 $m/s$ |

# 3 THEORETICAL ASSUMPTIONS AND THEIR SIGNIFICANCE

1. The fluid (air) is assumed to be under the continuum regime and all properties are assumed to be point-wise continuous as per the Continuum Hypothesis.

2. The flow past the airfoil is assumed to be predominantly dominated by inertial effects rather than viscous effects (momentum diffusion). This assumption is justified by the fact that the Reynolds' Number ($R_e$) is large (164282.97).

3. The airfoil is assumed to have small thickness and thus perturb the flow minimally. This is apparent from the fact that maximum thickness is only 12 % of chord in the particular experimental setup. This simplifies the expression for axial and normal force coefficients as we are able to neglect the second order terms in Eqn. 8. Also the above assumption also takes into consideration that and the angle of attack is small *(−4° to +6°)*. But we are not using this assumption while deriving the sectional coefficients of lift, drag and aerodynamic moments in Eqns. 13, 14 and 12. These assumptions allow us to use the expressions for force and moment coefficient from Thin Airfoil Theory.

4. The flow past the airfoil is assumed to be within the incompressible regime as the Mach number of the flow is small *(M = 0.0498)* this corresponds to simplification of conservation laws employed for mass and momentum into Eqns .

5. Integrals computed using trapezoidal rule are reasonably accurate.

# 4 PROCEDURE

## 4.1 Measurement of Airfoil Surface Pressure Distribution

1. The ambient conditions (ambient temperature and pressure) are noted to calculate the density of air before the experiment. Using the calculated density, the required dynamic pressure corresponding to specified velocity is calculated.
2. The wind tunnel and the airfoil are inspected to for any leaks or clogged ports. If present, any leaks in the wind tunnel are closed and the data from clogged ports are neglected.
3. The frequency of the motor is set to achieve required dynamic pressure (measured through Pitot probe located away from the airfoil) corresponding to the required velocity. Once the frequency is set, the motor is left undisturbed.
4. The 30 tubes from the pressure ports on the airfoil (15 of upper surface, 15 of lower surface) are connected to the channel boxes for pressure readings.
5. The required angle of attack is set on the spirit level and the airfoil is rotated such that the spirit level is indicator is between the two level markers.
6. The gauge pressure is noted for each port twice for repeatability and entered into the test matrix. MS Excel is used to tabulate the test matrix.
7. The above steps are repeated for all values of $\alpha$ in the test matrix. For the current instance of the experiment, $\alpha$ range between $-4°$ and $+6°$ is taken with values at $-2°$, $0°$ and $+4°$ degrees.

## 4.2 Measurement of Airfoil Wake Velocity Profile

1. The Pitot tube is placed aft of the airfoil above its immediate wake by moving it in the x direction along the traverse.
2. The Pitot tube is inspected and ensured to be aligned along free stream flow direction.
3. The Pitot tube is moved along the y direction in small increments and two values of the dynamic pressure head measured by the Pitot tube is noted at each y location for repeatability.
4. Repeat both these measurements for different angles of attack ($-4°$ to $+6°$)

# 5 EXPERIMENTAL CALCULATIONS

## 5.1 Sample calculation approach

Using the $C_p$ distribution obtained from wind tunnel experiment and the airfoil coordinates corresponding to the locations of pressure ports, the axial and normal force coefficients (sectional) are computed using the Eqns. 11, 10.

The sectional lift and pressure (form) drag coefficients as well as the leading edge moment coefficient are computed from the data of axial and normal force coefficients using the Eqns. 13, 14 and 12.

Note : The simplification of the expression for lift and drag coefficients using for small incidence angles is not considered for greater accuracy.

The sectional coefficient of moment about quarter-chord point and an estimate of aerodynamic center are calculated using the Eqns. 15 and 16.

Using the velocity profile in the airfoil wake, the sectional total drag coefficient is computed using the Eqn. 17.

From the calculated values of sectional coefficients of pressure and total drag, the skin-friction drag coefficient can be computed as follows:

$$C_{d,f} = C_{d,total} - C_{d,p} \tag{25}$$

## 5.2 Tabulated calculations

| $\alpha$(°) | -4 | -2 | 0 | 4 | 6 |
|---|---|---|---|---|---|
| $C_{l,theory}$ | -0.4386 | -0.2193 | 0.0000 | 0.4386 | 0.6580 |
| $C_{l,exp}$ | -0.4718 | -0.3602 | -0.0066 | 0.4505 | 0.6719 |
| $C_{m,LE,theory}$ | 0.1097 | 0.0548 | 0.0000 | -0.1097 | -0.1645 |
| $C_{m,LE,exp}$ | 0.1221 | 0.0788 | -0.0289 | -0.1405 | -0.1947 |
| $C_{m,c/4,theory}$ | 0 | | | | |
| $C_{m,c/4,exp}$ | 0.1043 | 0.0652 | -0.0291 | -0.1235 | -0.1694 |
| $x_{cp,theory}/c$ | 0.25 | | | | |
| $x_{cp,exp}/c$ | 0.2574 | 0.2179 | -4.3536 | 0.3102 | 0.2883 |

**Table 1:** Comparison Table with theoretical data

| $\alpha$(°) | -4 | -2 | 0 | 4 | 6 |
|---|---|---|---|---|---|
| $C_{d,total}$ (XFLR5) | 0.0844 | 0.0771 | 0.0802 | 0.0830 | 0.1067 |
| $C_{d,total}$ | 0.1144 | 0.0817 | 0.0941 | 0.1171 | 0.1391 |
| $C_{d,pressure}$ (XFLR5) | 0.0378 | 0.0379 | 0.0444 | 0.0372 | 0.0524 |
| $C_{d,pressure}$ | 0.0543 | 0.0478 | 0.0269 | 0.0479 | 0.0670 |
| $C_{d,skinfriction}$ (XFLR5) | 0.0466 | 0.0391 | 0.0359 | 0.0458 | 0.0543 |
| $C_{d,skinfriction}$ | 0.0601 | 0.0339 | 0.0672 | 0.0693 | 0.0721 |

**Table 2:** Drag Comparison Table with XFLR5 data

# 6 RESULTS

## 6.1 Plots

### 6.1.1 Representative $C_p$ Plots

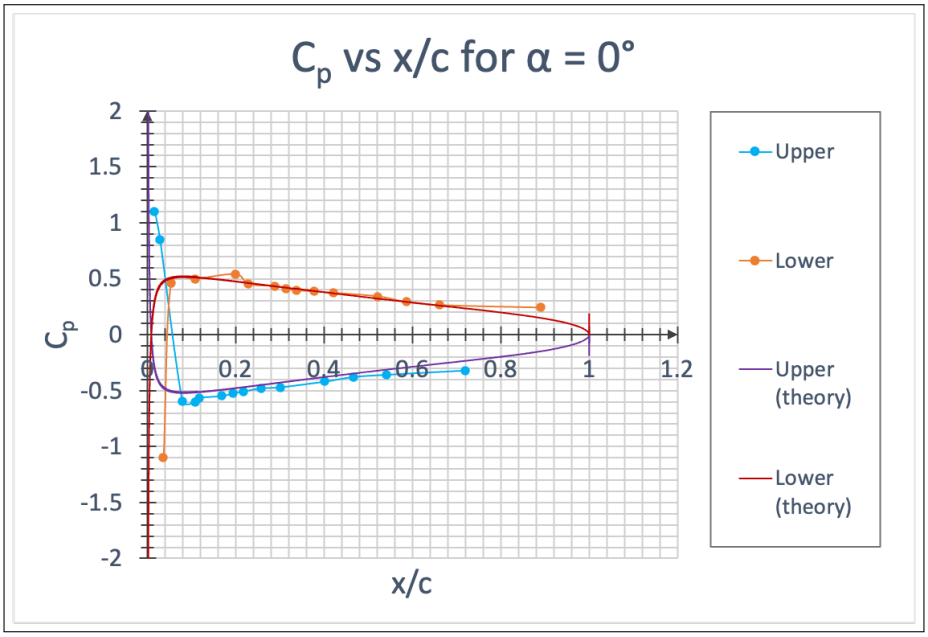


**Figure 7:** $C_p$ vs x/c for $\alpha$ = 0°

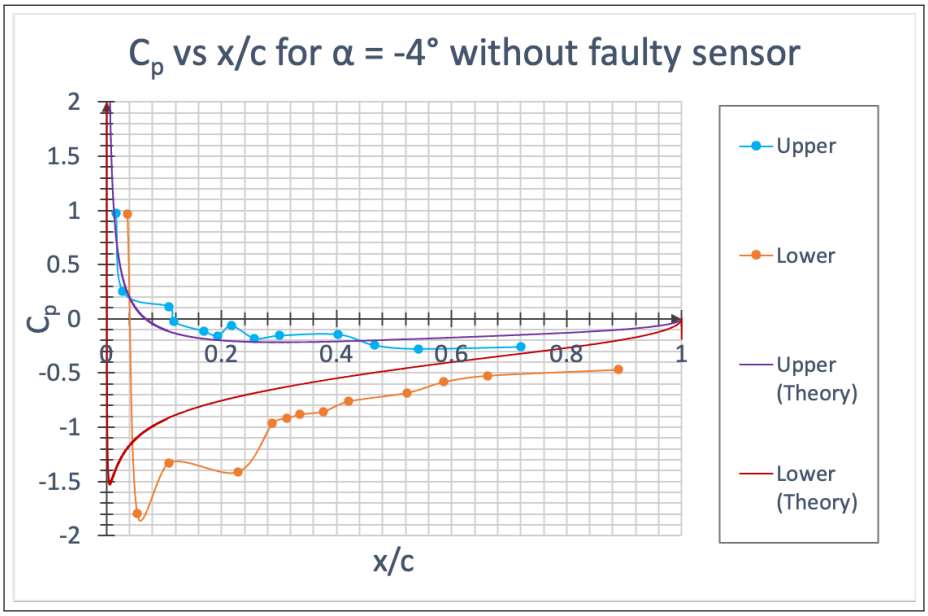


**Figure 8:** $C_p$ vs x/c for $\alpha$ = -4° (after neglecting faulty sensor data)

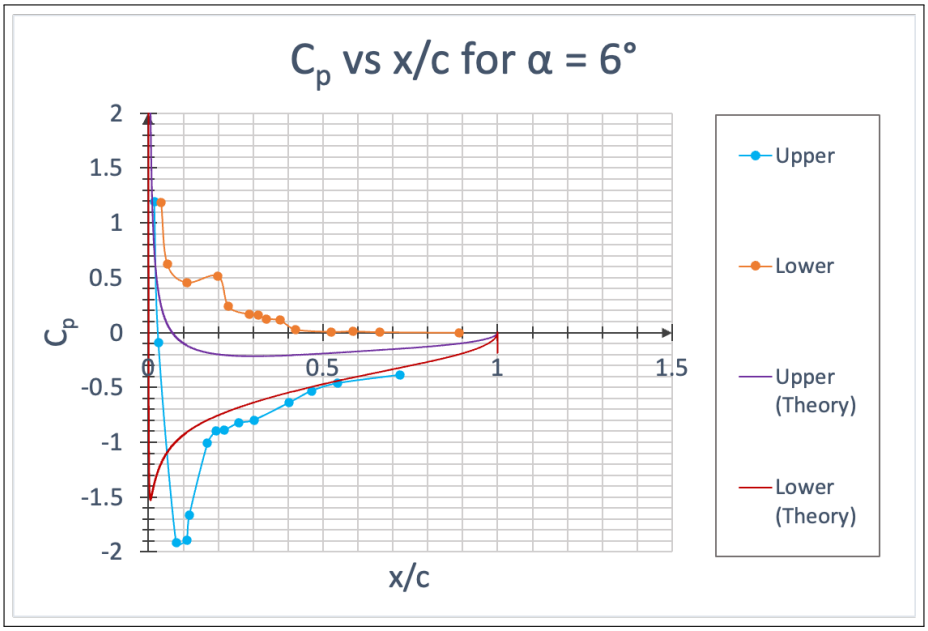


**Figure 9:** $C_p$ vs x/c for $\alpha = 6°$

### 6.1.2 Representative Wake Velocity Profile

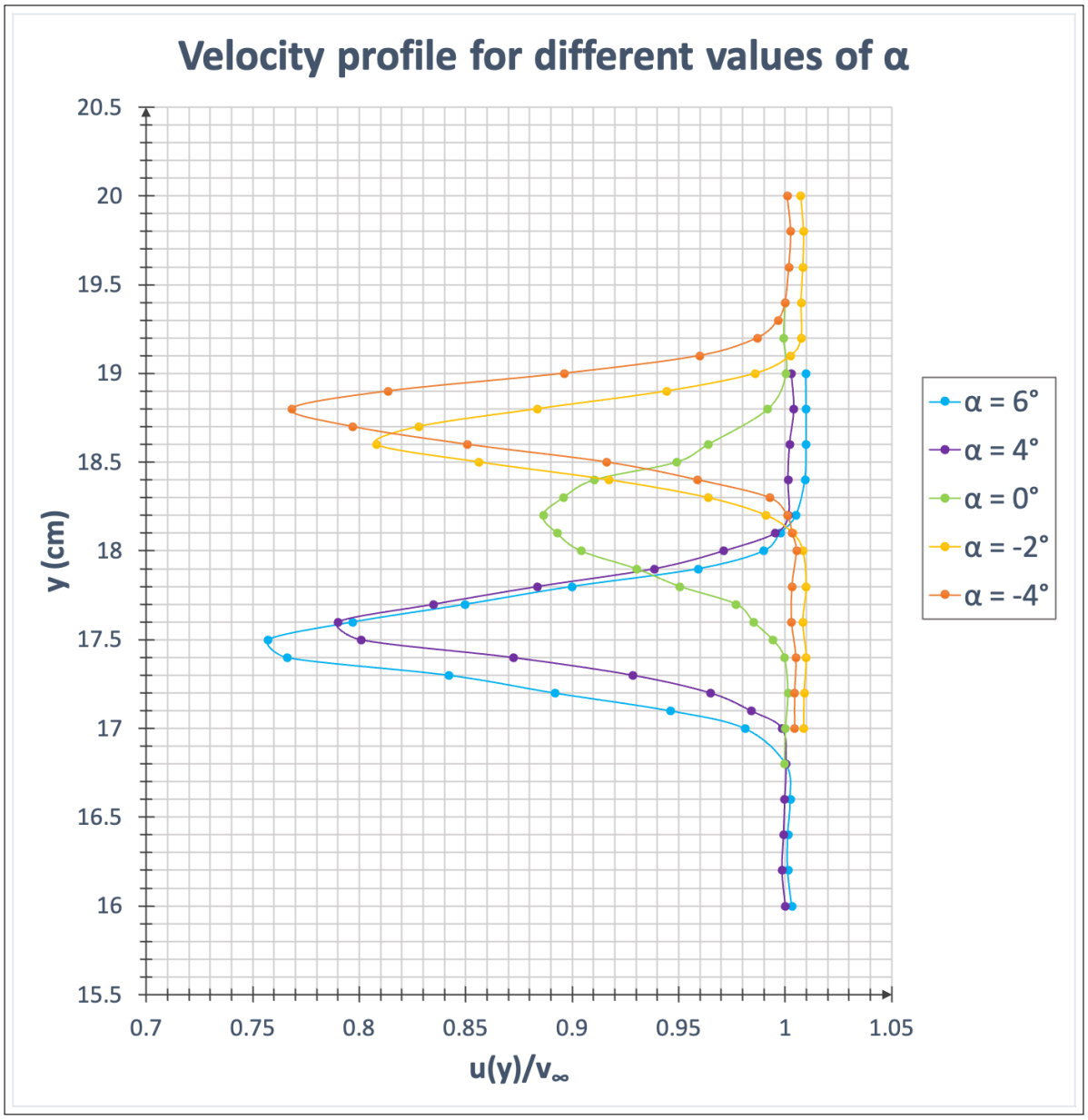


**Figure 10:** Wake Velocity Profile for various $\alpha$

## 6.2 Comparison with Literature and Theoretical Data

### 6.2.1 Lift Coefficient ($C_l$) vs $\alpha$

The plots for $C_l$ vs $\alpha$ obtained from wind tunnel is shown in Figure 11. It is compared with theoretical values obtained by using Eqn. 26 from Thin Airfoil Theory and also the data obtained from the computational software XFLR5 for the Reynolds' number of 162225 obtained using the chord length as characteristic length

$$C_{l_{theo}} = 2\pi\left[\alpha + \frac{1}{\pi}\int_0^{\pi}\frac{dz}{dx}(\cos(\theta_o)-1)d\theta_o\right] \tag{26}$$

$$\Rightarrow C_{l_{theo}} = 2\pi[\alpha], \text{ where} \alpha \text{ is in radians} \tag{27}$$

$$\Rightarrow C_{l_{theo}} = 0.1097\alpha, \text{ where} \alpha \text{ is in degrees} \tag{28}$$

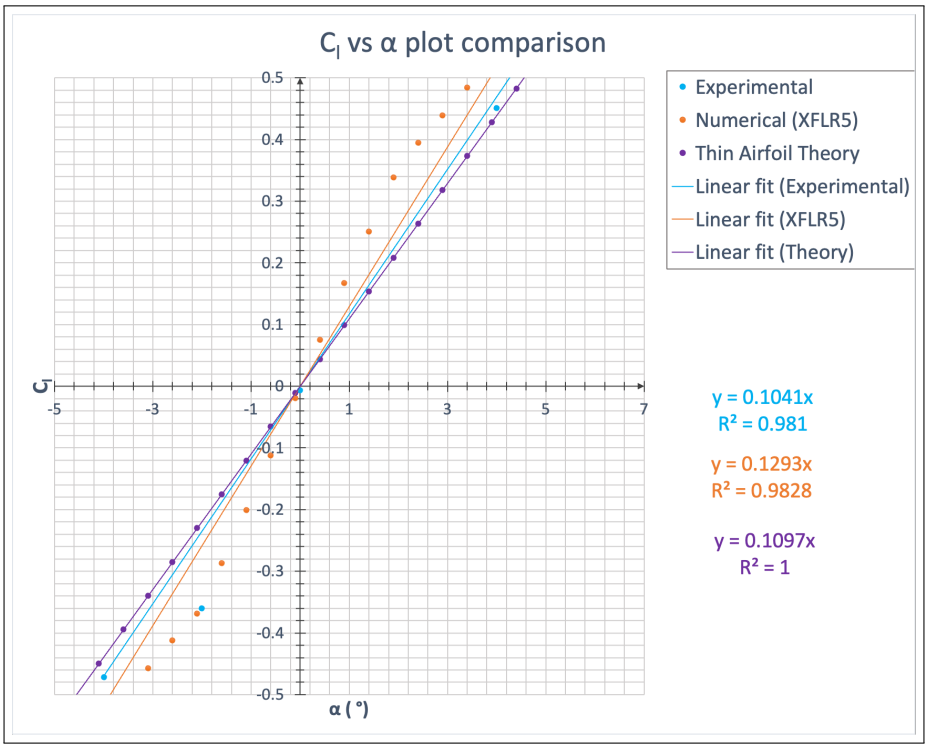


**Figure 11:** $C_l$ vs. $\alpha$ comparison with theoretical and numerical data

### 6.2.2 Drag Coefficients ($C_{d,}$) vs $\alpha$

The plots of $C_{d,pressure}$, $C_{d,skinfriction}$ and $C_{d,total}$ vs $\alpha$ obtained from wind tunnel is shown in Figure 12, Figure 13 and Figure 14 respectively. It is compared with numerical values obtained from the software XFLR5[4]. Since theoretical results for drag calculation require knowledge of theoretical pressure distribution in airfoil wake, it is omitted and instead a validation is done for $\alpha = 0°$ for similar Reynolds' number from literature[7].

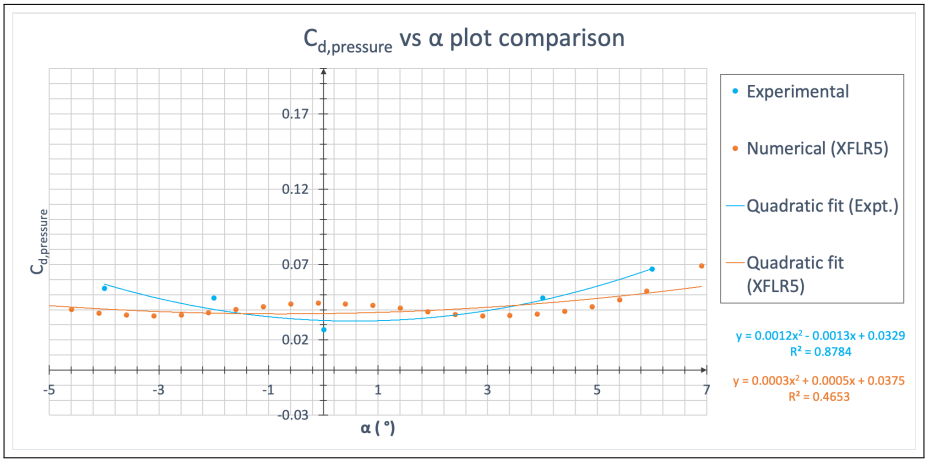


**Figure 12:** $C_{d,p}$ vs. $\alpha$ comparison with numerically computed values

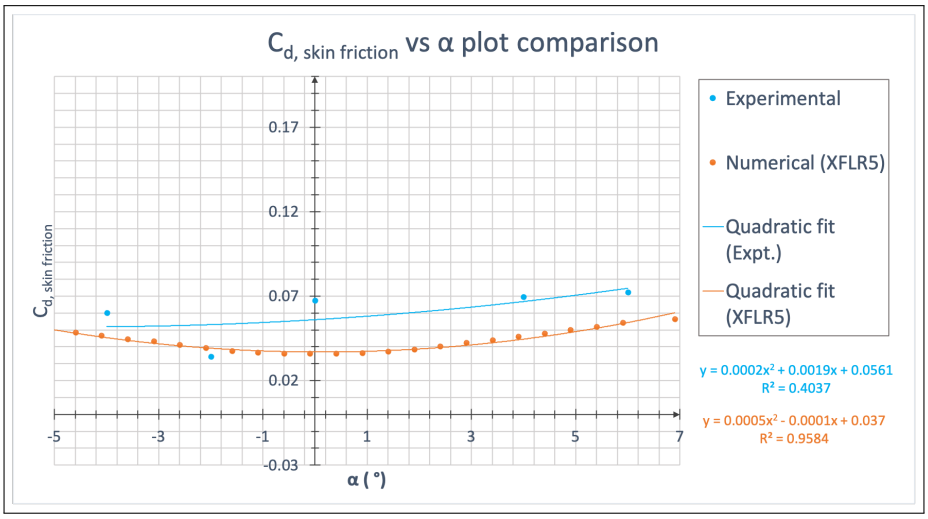


**Figure 13:** $C_{d,sf}$ vs. $\alpha$ comparison with numerically computed values

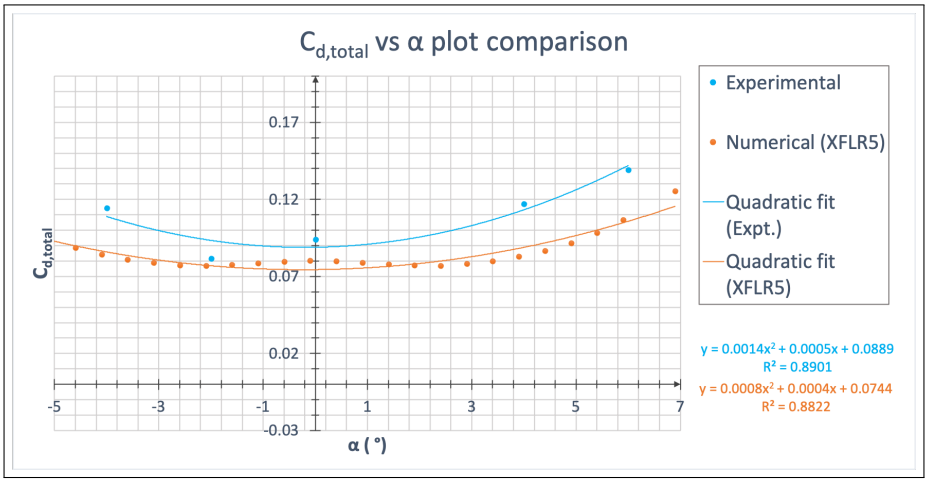


**Figure 14:** $C_{d,total}$ vs. $\alpha$ comparison with numerically computed values

### 6.2.3 Moment Coefficients $(C_{m,})$ vs $\alpha$

From Eqns. 22, and 12 the values for theoretical and experimental values of sectional moment coefficients about leading edge are obtained:

$$C_{m,LE_{theo}} = -0.02742\alpha$$

$$C_{m,c/4_{theo}} = 0$$

$$C_{m,LE_{exp}} = -0.033\alpha$$

$$C_{m,c/4_{exp}} = -0.286\alpha$$

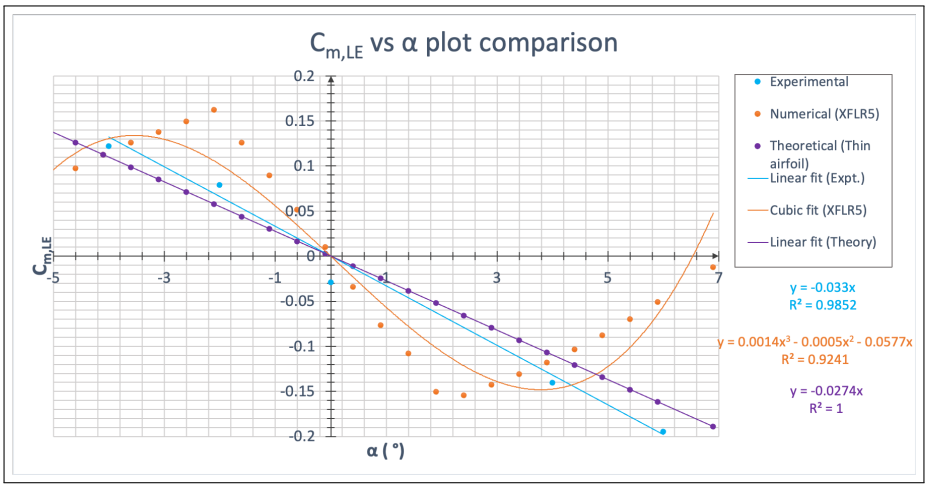


**Figure 15:** $C_{m,LE}$ vs. $\alpha$ - experimental

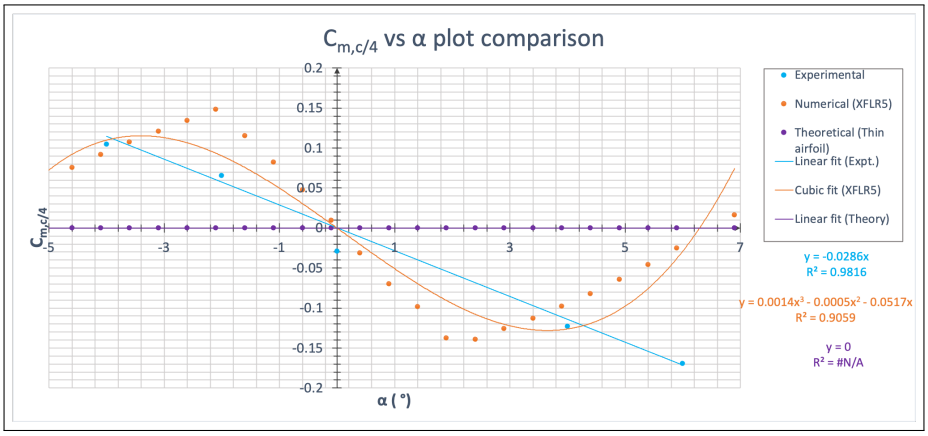


**Figure 16:** $C_{m,c/4_{theo}}$ vs. $\alpha$ - experimental

### 6.2.4 Center of pressure $(x_{cp})$ vs $\alpha$

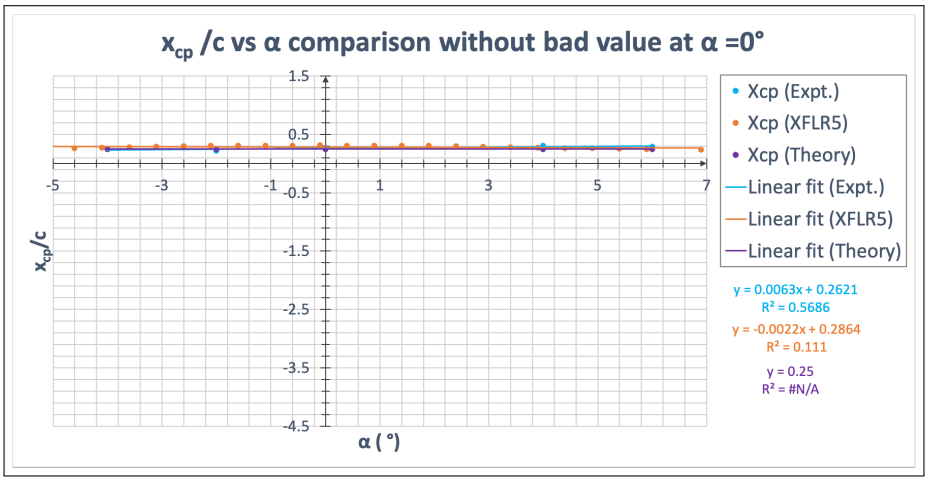


**Figure 17:** $x_{cp}$ vs. $\alpha$

## 6.3 Estimation of Stall Angle

The variation for $C_l$ for range of $\alpha$ values is linear. Hence the stall angle cannot be found using this data. So the XFLR5 data is used to find the stall angle $(\alpha_{stall})$. The domain of $\alpha_{stall}$ can be estimated as the region where $\frac{dC_l}{d\alpha}$ changes sign from +ve to -ve.

Here the $\alpha_{stall}$ is close to 11°as seen in the plot below Fig18.

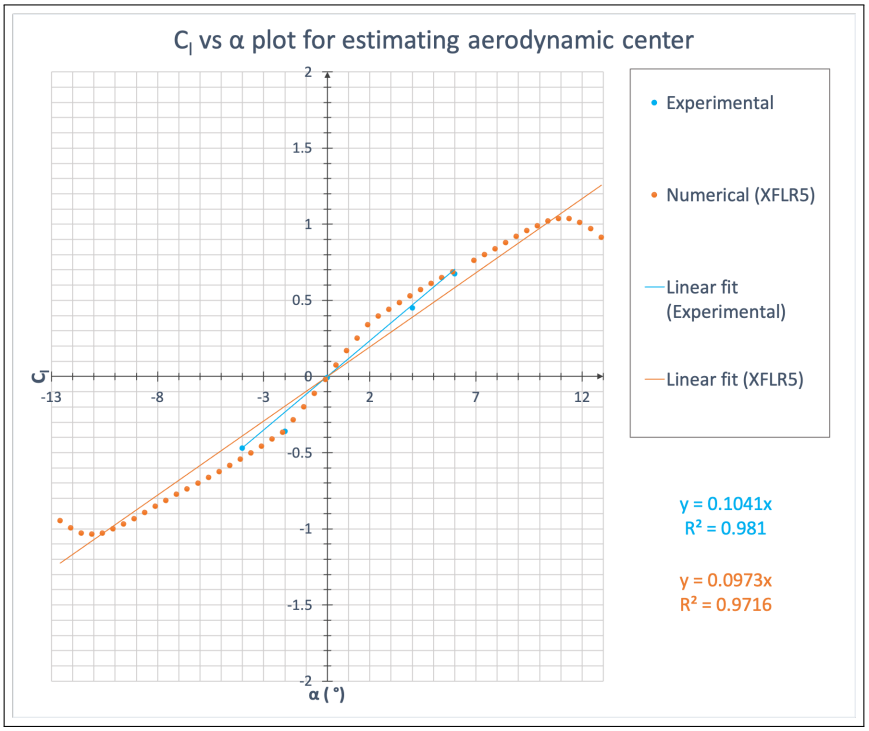


**Figure 18:** $C_l$ vs. $\alpha$

## 6.4 Estimating Location of Aerodynamic Center

$$\frac{x_{ac}}{c} = -\frac{m_o}{a_o} + 0.25 \tag{29}$$

where

$$\frac{m_o}{a_o} = \frac{dC_{m,c/4}}{dC_l} = \frac{dC_{m,c/4}/d\alpha}{dC_l/d\alpha} \tag{30}$$

From the experimental data the value of $\frac{x_{ac,exp}}{c} = 0.4857$ is obtained after averaging for all $\alpha$, whereas $\frac{x_{ac,theory}}{c} = 0.25$ as the theoretical aerodynamic centre for all symmetric airfoils is its quarter chord point.

## 6.5 Error Analysis (correct significant digits)

The below are the sources of errors due to least count of measurement devices:

1. There is an error of 0.01 millibar in barometer (4 significant digits)
2. There is an error of 0.1 K in the thermometer (3 significant digits when expressed in Kelvin)
3. The manometer reading carry an error of 0.1 pascal (3 significant digits)
4. The screw gauge used to obtain airfoil coordinates have an error of 10 $\mu$m (2 significant digits when expressed in mm for y-coordinate and 4 significant digits for x-coordinates in mm)

We use the following relations for error analysis and propagation of arithmetic errors:

1. for

$$z = x \pm y \tag{31}$$

$$\Delta z = \sqrt{(\Delta x)^2 + (\Delta y)^2} \tag{32}$$

2. for

$$z = x * y \quad \text{or} \quad x/y \tag{33}$$

$$\frac{\Delta z}{z} = \sqrt{\left(\frac{\Delta x}{x}\right)^2 + \left(\frac{\Delta y}{y}\right)^2} \tag{34}$$

Taking $C_p = \frac{P}{0.5 \times \rho V_\infty^2}$, relative error in $\rho$ is $7.97 \times 10^{-2}$. Thus the relative error in $C_p$ is $\pm 9.3 \times 10^{-2}$. According to the respective calculations the relative error in $C_a$ and $C_n$ is $\approx 9.4 \times 10^{-2}$. Then the relative error that is propagated to $C_l$ is $\approx 1.4$ for $\alpha = 0$ case and $\approx 0.3 \times 10^{-2}$ assuming that alpha is taken up to 4 significant digits or more for other cases. Similarly the error in $C_{m,le}$ is $\approx 7.3 \times 10^{-2}$ and the error in $C_{m,c/4}$ is $\approx 4.1 \times 10^{-2}$.

The percentage error between the calculated values of the aerodynamic center and the predicted values from Thin Airfoil Theory comes out as 94.28%

Apart from this, the curve fitting is observed to have a high correlation factor ($R^2$) and the result matches closely with theoretical and numerical plots.

### 6.6 Tabulated dependence on angle of attack and RMS errors

The table below contains the assumed parametric dependence of the airfoil parameters with angle of flow incidence $\alpha$ (in degrees) obtained from the plots. The RMS error of the assumed fit from actual values is also calculated for each parameter.

| Quantity | Parametric dependence on $\alpha$ | RMS error |
|---|---|---|
| $C_l$ | $0.1041\alpha$ | 0.0770 |
| $C_{d,pressure}$ | $0.0012\alpha^2 - 0.0013\alpha + 0.0329$ | 0.0046 |
| $C_{d,skinfriction}$ | $0.0002\alpha^2 - 0.0019\alpha + 0.0561$ | 0.0179 |
| $C_{d,total}$ | $0.0014\alpha^2 - 0.0005\alpha + 0.0889$ | 0.0076 |
| $C_{m,LE}$ | $-0.0330\alpha$ | 0.0153 |
| $C_{m,c/4}$ | $-0.0286\alpha$ | 0.0148 |
| $x_{cp}/c$ | $-0.0063\alpha + 0.2621$ | 2.0686 |
| $x_{ac}/c$ | Assumed independent of $\alpha$ | 0.2357 |

**Table 3:** Table for errors and parametric dependence on $\alpha$

# 7 CONCLUSIONS & DISCUSSION

### 7.1 Comparison between plots

From the plots of $C_p$ vs $x$ the following can be inferred:

1. The $C_p$ data agrees closely with that predicted from Thin Airfoil Theory for $\alpha = 0°$ but diverges from predicted values for higher values. This can be associated with the underlying assumption that the airfoil is thin is not accurate in case of the actual airfoil experiment as observed pressure heads are more than that predicted by thin airfoil theory. But one can easily observe the physical trends in the plots as the pressure head at the suction surfaces increase with flow incidence angles. This is seen in case of higher pressure head in case of $\alpha = 6°$ plot compared to that of $\alpha = -4°$ plot. Also the suction surface and pressure surfaces are interchanged for a negative incidence angle agreeing with physical interpretations of pressure distribution on airfoil surface.

2. The data of velocity profile matches accurately with the expected data from literature[3] as shown by Figure19. The small deviations can be attributed to the losses due to tunnel leakage. The velocity profile also follows expected trends with varying angles of attack.

Higher angles of incidence gives higher wake velocity and usually a longer wake. Also wake velocity peak shifts up or down corresponding to negative and positive values of the flow incidence angles as observed by the Figure 10

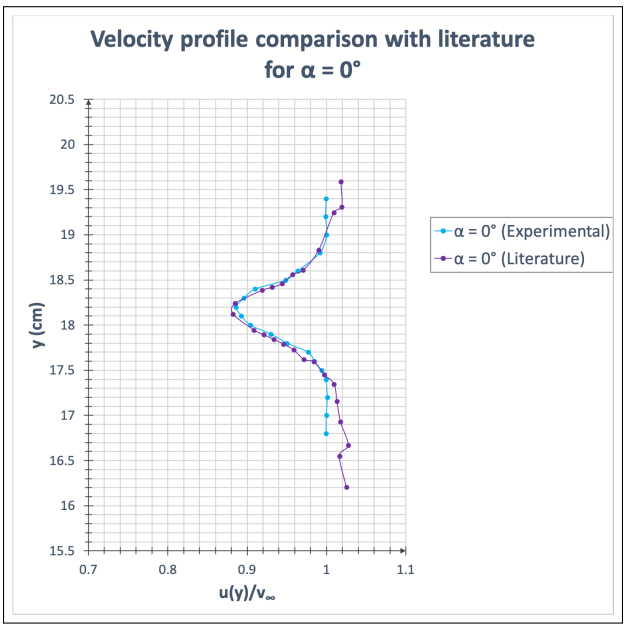


**Figure 19:** Velocity profile in wake vs. z comparison with literature

3. The values of $C_{m,LE}$ and $C_{m,c/4}$ are not in agreement with the numerical data as the numerical solver does not use the linear dependence of these moments with $\alpha$ suggested by Thin Airfoil Theory. Nevertheless, assuming linear dependence is reasonable for small angles of attack as seen from the linear region present between $\alpha = \pm 1°$. Beyond this range, the effect of thickness of the airfoil and non-minimal flow perturbation results in deviation from the linear dependence.

4. A very interesting observation is made with the value of $x_{cp}$ at zero angle of incidence as it is nowhere near the numerically computed or theoretically predicted values. This is due to the nature of symmetric airfoils that center of pressure is indeterminate from the moment ($C_{m,LE}$ and lift ($C_l$ coefficients (or coefficient of normal force ($C_n$ to be precise) as they both approach zero as $\alpha$ approaches zero. Thus the value of $x_{cp}$ obtained from experiment is inherently wrong and thus can be neglected. This omission is applied while plotting the curve for $x_{cp}$ vs $\alpha$ and it was observed that upon omission of $x_{cp}$ value at zero angle of incidence the experimental plot agrees more with theoretical and numerical values. The plot without neglecting the $x_{cp}$ value at $\alpha = 0$ is shown in Figure 20 for comparison with the plot presented in Figure 17.

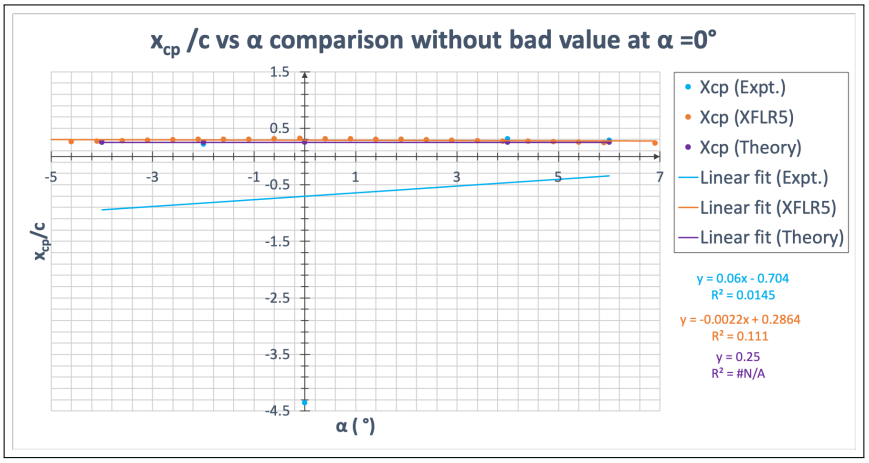


**Figure 20:** $x_{cp}$ vs. $\alpha$ plot without omitting value at $\alpha = 0$

5. There is also the issue of faulty pressure sensor data due to clogged pressure ports at some locations. These values are identified and omitted for $C_p$ distribution plots and further calculations. One such case is denoted below for the $C_p$ vs $x/c$ plot for $\alpha = -4°$ shown in Figure 21 for comparison with the better data obtained after omitting the faulty sensor given in Figure 8

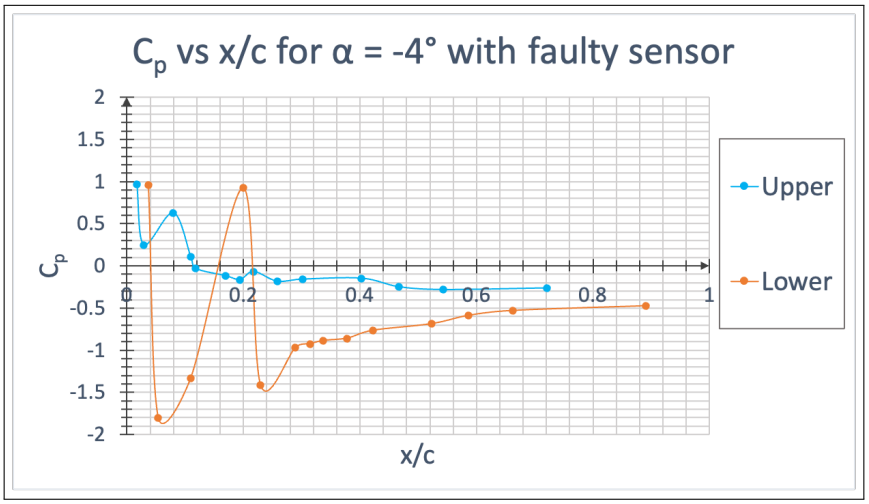


**Figure 21:** $C_p$ vs. $x/c$ plot without omitting value at pressure port 4

6. The value of aerodynamic center comes out to be about halfway of chord length as opposed to the prediction from Thin Airfoil Theory that it lies at quarter chord point. This fact is solely due to the fact that thin airfoil theory assumes that the airfoil is thin and neglects the effect of thickness at high angles of attack. Also,it can be noted that the values predicted from Thin Airfoil Theory are not in agreement from experimentally data

obtained from literature[7] from a very reliable source. Thus we can take confidence in the fact that the airfoil does not deviate from the physical behaviour expected and it is the theory that has failed to capture realistic behaviour due to over-simplification.

# References


[1] Airfoiltools.com. airfoil tools, 2023.

[2] John D. Anderson. *Fundamentals of Aerodynamics*. McGraw-Hill, Inc., second edition, 1991.

[3] Mehdi. Banafi and Mehrdad. Banafi. An experimental research on wake behind airfoil naca 0012 under various angles. *International Journal of Theoretical and Applied Mechanics*, 2, 2017.

[4] B. H. Carmihael. guidelines on xflr5 for analysis of foils and wings operating at low reynolds numbers, 2009.

[5] UIUC Department of Aerospace Engineering. airfoil coordinates database, 2023.

[6] Arnold M. Kuethe and Chuen-Yen Chow. *Foundations of Aerodynamics: Bases of Aerodynamic Design*. John Wiley Sons, Inc., fifth edition, 1998.

[7] NACA. technical note of naca 0012 airfoil, 1955.

[8] Prof. Vineet Nair. Airfoil laboratory briefing. Department of Aerospace Engineering, 2023.

[9] Prof. Aniruddha Sinha. Lecture slides of ae 333 (aerodynamics). Department of Aerospace Engineering, 2022.

[10] XFLR.tech. xflr5 documentation file, 2009.